Electrochemical characterization of ZrTi alloys for biomedical applications. Part 2. The effect of thermal oxidation

Georgiana Bolat[1], Javier Izquierdo[2], Ricardo M. Souto[2], Daniel Mareci[1]

[1]Faculty of Chemical Engineering and Environmental Protection, ''Gh. Asachi'' Technical University of Iasi, B-dul D. Mangeron, nr. 59, 700050 Iasi, Romania.
[2]Department of Physical Chemistry, University of La Laguna, E-38205 La Laguna (Tenerife, Canary Islands), Spain

Abstract:

Oxidation in air of ZrTi alloys at 500 ºC for 2 h produces oxide-covered materials with a very high corrosion resistance in Ringer's solution at 37 ºC. The oxide layers present a double-layer structure, comprised by a thin and very compact inner layer of ca. 5 nm thickness, and a less compact, more porous and thicker outer layer. The thickness of the outer layer greatly varies with the composition of the base ZrTi alloy, but has very little influence in the overall electrochemical behaviour of the material. The nature of the oxide layer is a mixture of ZrO_2 and TiO_2, and no evidence of higher oxidation states of the metal could be found using XRD data. Anodic dissolution through the passive layers formed on the oxidized alloys is greatly diminished compared to those measured from the untreated materials, allowing all the alloying ratios between Zr and Ti to be potentially considered for implant application. The combination of alloying with titanium and oxidation in air at 500 ºC resulted in the materials that do not exhibit the characteristic susceptibility of zirconium towards the initiation of localized corrosion processes in aqueous chloride-containing electrolytes even for anodic polarizations up to +1.00 V_{SCE}, a value well above the highest polarization experienced in the human body. Though all the oxidized alloys exhibited remarkable corrosion resistances, the best behaviour was found for oxidized Zr45Ti.

Keywords: ZrTi alloys; thermal oxidation; oxide films; corrosion resistance; impedance spectroscopy; biomaterials.

1. Introduction

It was shown in part 1 of this publication that alloying zirconium with titanium offers an attractive biomaterial alternative [1] for the replacement of commonly-employed titanium-based materials that contain toxic and allergenic elements such as vanadium and aluminium [2-5]. Though titanium and its alloys spontaneously passivate in air and in aqueous electrolytes with the formation of adherent and stable oxide films [6-8], they are susceptible to pitting corrosion in chloride-containing media [7,9-12] with the result that metal ions may be released to the surrounding tissues [5,13-16]. Zirconium is considered to be non-toxic and non-allergenic [17], and it stabilizes the β-phase of titanium [17]. It has been reported that zirconium influences the stability of passivating oxides and hinders the activation of metallic titanium exposed to reducing acids [18]. This effect has been justified by invoking that zirconium is a strong oxide former and likely produces Zr-O bonds of high strength [19]. Unfortunately, zirconium is susceptible to localized corrosion induced by chloride ions too [20,21]. In contrast, the addition of titanium to zirconium reduces the susceptibility of the later towards localized corrosion, and the passive films developed by the ZrTi alloys provided a more insulating barrier towards electron transfer at the surface of the alloys compared to Ti when the oxide layers were spontaneously formed at their corresponding OCP values during immersion in Ringer's physiological solution [1]. But this protective effect could not be effectively maintained in ZrTi alloys with titanium contents smaller than 45 wt.% subjected to anodic polarization at potential values achieved in the human body [22] due to thickening and eventual breakdown of the passive oxide layers due to hazardous localized corrosion phenomena.

Surface modification treatments can greatly improve the passivation characteristics of oxide layers on titanium-based materials [23]. In particular, high-temperature oxidation of metals and alloys leads to the rapid formation of oxide films on their surface, and they usually exhibit a multilayer structure [24,25]. This effect has been documented for high-temperature oxide films on a stainless steel surface [26], and the electrical resistive and capacitive properties were correlated with the oxidation parameters. The same effect was described for Ti-48Al-2Cr-2Nb alloy that produced a porous oxide layer when oxidized at 800 ºC in air, whereas surface oxidation at 500 ºC significantly increased the corrosion of γ-TiAl [27]. Being corrosion products, high-temperature oxide films may present a distribution of defects, which may facilitate the penetration of the electrolyte into the passive film and consequently decrease the corrosion protection provided by the oxide layer [28,29].

It is the aim of the second part of this publication to investigate the corrosion behaviour of air-oxidized ZrTi alloys in Ringer's solution, used to simulate body fluids, at 37 ºC. Electrochemical characterization was performed using linear potentiodynamic polarization (LPC) and electrochemical impedance spectroscopy (EIS) techniques with the objective to determine the potential ranges for the stability of the materials, and to quantify the resistance of the passive films developed on them. The formation of surface oxide layers with enhanced barrier characteristics would imply that ZrTi alloys can be considered as a biomaterial.

2. Experimental

Three different ZrTi alloys, all produced by Zirom S.A. (Giurgiu, Romania), were considered in this investigation. The chemical composition of each material is given in Table 1. Samples were ground to a finish of 2000 grit with silicon carbide paper, ultrasonically cleaned in twice-distilled water, degreased in ethanol, and dried in air. The samples were then oxidized in air at 500 ºC for 2 h.

The test electrolyte was naturally-aerated physiological Ringer's solution at 37 ± 1 ºC. Ringer's solution was made to composition 8.6 g L^{-1} NaCl, 0.3 g L^{-1} KCl, and 0.48 g L^{-1} $CaCl_2$, in twice-distilled water. The pH of this solution was 6.8.

A three-electrode corrosion flow cell kit (C145/170, Radiometer, France) with platinum as counter electrode and saturated calomel reference electrode (SCE) as reference electrode was employed for all the electrochemical measurements. The electrochemical cell contained a freely adjustable Luggin capillary to house the reference electrode. The sample was mounted in a PCTFE sample holder so that the exposed surface of the oxidized alloys to the test electrolyte was a disc of 0.95 cm^2. All the potentials in this paper are referred to the SCE.

All electrochemical measurements were carried out on a Princeton Applied Research potentiostat Model PARSTAT 4000 (Princeton Applied Research, Princeton, NJ, USA). The instrument was controlled by a personal computer and specific software (VersaStudio, PAR, Princeton, NJ, USA). Measurement of linear potentiodynamic polarization curves (LPC) was initiated after 24 h exposure to the test environment. The potential was initiated at a potential value 0.20 V negative to the corresponding open circuit potential of the sample in the solution, and it was extended in the positive direction up to +1.00 V_{SCE}, at a sweep rate of 1 mV s^{-1}. The linear potentiodynamic polarization curves

were plotted, and the corresponding values for the open circuit potential (E_{corr}), the corrosion current density (j_{corr}), and the passivation current density (j_{pass}), were determined from them.

Electrochemical impedance spectroscopy (EIS) measurements were also performed using the same instrumentation. The perturbation amplitude was 10 mV and the frequency ranging from 100 kHz down to 1 mHz. Ten points were recorded for each frequency decade. The EIS spectra were obtained at different times after the electrode was immersed in the Ringer's solution. The EIS experimental data were analyzed in terms of equivalent circuits (EC) using *ZSimpWin 3.22* software [30].

All electrochemical tests begun with a new sample, and they were repeated three times to ensure reproducibility of the measurements.

The morphology of the oxidized ZrTi alloys, both before and after the electrochemical tests, was observed by scanning electron microscopy (SEM) using a Quanta 3D Model AL99/D8229 (FEI, Hillsboro, OR, USA) operating with beam energy 30 kV. In addition, the elemental analysis of the surfaces was done by energy dispersive X-ray spectroscopy (EDS).

X-ray diffraction (XRD) spectra were employed for the identification of oxides formed on the surface of the oxidized ZrTi samples. XRD spectra were recorded using an X'Pert PRO MRD (PANalytical, city, Holland) diffractometer equipped with a Cu Kα anode, and the XRD patterns were scanned in the $20 \leq 2\theta \leq 90$ degrees range at a rate of 1.5 degree min^{-1}.

3. Results

3.1. Electrochemical characterization.

Linear potentiodynamic polarization techniques were employed to establish the potential ranges of the different electrochemical reactions occurring during the anodic polarization of oxidized ZrTi alloy specimens. The polarization curves recorded at a sweep rate of 1 mV s^{-1} in Ringer's solution at 37 ºC are plotted in Figure 1. Potential limits were defined between 0.20 V negative to their corresponding open circuit potential attained after 24 h immersion in the test environment, and +1.00 V_{SCE}, a positive potential value 0.50 V more positive than the highest value recorded in the human body until now [22]. None of the three oxidized ZrTi alloys showed an active region in the linear polarization plots following the Tafel region but they entered directly into a stable passive regime. And the passive region extended

over the whole complete range of potentials up to the anodic limit considered in this work. No rapid increases in the anodic current were observed that could be related to passivity breakdown as result of localized corrosion or transpassive processes. Therefore, breakdown potentials, E_b, are well above the range of potential the metals can experience in open circuit for all the samples tested. Therefore, the oxide layers formed on the surface of ZrTi alloys at 500 ºC render these alloys passive and highly corrosion resistant in Ringer's solution at temperatures around those experienced in the human body.

For the sake of comparison, the polarization curves were also analyzed to extract the values for the corrosion potential (E_{corr}), corrosion current density (j_{corr}), and the passive current density (j_{pass}), and they are given in Table 2. The formation of oxide on the ZrTi samples, resulting from surface treatments renders the three metal alloys passive in Ringer's solution at 37 ºC. Yet some differences can be observed as corrosion and passivation current densities were found to depend on the alloy compositions. Oxidized Zr5Ti and Zr25Ti samples exhibited higher corrosion current densities than the oxidized Zr45Ti sample, possibly due to the presence of more porous mixed TiO_2/ZrO_2 layer. And the passivation current densities determined for the Zr25Ti and Zr45Ti samples were approximately one order of magnitude smaller than that determined for the Zr5Ti sample. These results indicate that some electrodissolution through the passive film takes place for the latter. That is, the surface of the oxidized Zr5Ti sample is more reactive towards electron transfer than the surfaces of oxidized Zr25Ti and Zr45Ti when subjected to anodic polarization conditions. A clear benefitial effect can be attributed to the presence of titanium in the binary alloy, as both lower passivation and corrosion current densities are observed for the Zr45Ti alloy.

The corrosion resistance and passivation characteristics of the oxidized alloys was quantified using electrochemical impedance spectroscopy (EIS). Impedance spectra were recorded for the oxidized Zr5Ti, Zr25Ti and Zr45Ti alloys exposed to Ringer's solution at 37 ºC for different elapsed times up to 1 week. The samples were always investigated at their spontaneously-developed open circuit potentials. The measured impedance spectra are shown in Figure 2 and they are displayed in the form of Bode diagrams. The advantages of this procedure are that the data for all measured frequencies are shown and a wide range of impedance values can be displayed simultaneously. The frequency dependence of the impedance modulus and the phase shift ϕ indicate whether one or more time constants are present in the system. From a cursory inspection of the spectra, it can be first observed that for a given material, they exhibited only very small changes with the elapse of time and they mainly occurred in the low-frequency region. The greater changes with time were exhibited by the oxidized Zr25Ti alloy. Secondly,

the spectra look quite different for the various ZrTi alloys after oxidation in air at 500 ºC. The spectra measured for oxidized Zr45Ti showed an extended frequency range of capacitive behaviour, characteristic of an effective barrier film, whereas oxidized Zr5Ti presented the narrowest capacitive regions. Therefore, the EIS spectra measured for oxidized ZrTi alloys and their variation with time of exposure demonstrate a significant influence of alloy composition on their electrochemical response during immersion in aerated Ringer's solution at 37 ºC.

Though the spectra for each of the materials can be easily distinguished among the plots, they all contain two time constants, and they could be satisfactorily analyzed using the same equivalent circuit (EC). Figure 3 shows the equivalent circuit, which is based on a two-layer model of an oxide film [31]. It assumes that the corrosion of the passive metal is hindered by an oxide film that acts as a barrier-type compact layer. The equivalent circuit consists of the combination of two parallel *RQ* elements in series with the resistance of the solution (R_{sol}) occurring between the sample and the reference electrode. Constant phase elements (CPE) were used instead of pure capacitances because of the non-ideal capacitive response due to the distributed relaxation feature of the passive oxide films, which could be observed as a depressed semicircle when the spectra were plotted in the corresponding Nyquist diagrams (not shown here). The impedance representation of CPE is given by:

$$Z_{(CPE)} = \frac{1}{Y_0 \, (j\omega)^n} \qquad (1)$$

where ω is the angular frequency and Y_0 is a constant, and the value of the exponent n indicates the deviation from ideal capacitive behaviour (e.g., when $n = 1$). The high frequency R_{ct} and $Q_{dl,}$ parameters describe the properties of the reactions at the oxide layer/solution interface, whereas in the low frequency range the parameters R_{ox} and Q_{ox} describe the resistance and the capacitance of the compact oxide layers. A very good correlation was obtained between EIS data using the proposed equivalent circuit and the experimental impedance spectra of the solution interface/oxide layer/alloy. Figure 2 provides an evidence of fitting quality when applied to the measured spectra because all the solid lines corresponding to the fitted spectra passed through the measured data (discrete points).

WARNING: There is a problem in relation to the evolution of impedance spectra with the duration of the immersion in Ringer's solution for all the alloys. Inspection of Figure 2 shows that steadily the impedance modulus decreases with time, thus leading to the Bode-modulus lines always running below those measured after 1 hour. This would be related to conductive pathways and pores in the oxide layer.

But the impedance parameters given in Table 3 show exactly the opposite trend. They increase 10 times after 1 week (!), and this means more compact layers with less pores. THIS MUST BE RESOLVED: PLEASE CHECK THE FITS!

Due to these 2 situations, I have written two alternate parts, one painted in yellow for the first case, and another in blue for the second. WE MUST CHOOSE ONE OF

Table 3 presents the corrosion parameters obtained for the three oxidized ZrTi alloys from the analysis of EIS data. Whereas charge transfer resistance values, $R_{ct,}$ in the range of kΩ cm^2 were determined for all the materials significantly higher values were obtained for the resistance of the oxide layers R_{ox} (they are quantified in MΩ cm^2). These results indicate that the corrosion protection of oxidized ZrTi samples is due to their oxide layer. And the values of both resistance parameters greatly increased with the elapse of time during the exposure of the samples to Ringer's solution though they were left at their spontaneously-developed open circuit conditions, i.e. no polarization was applied to the systems. A significant effect related to aging of the oxide layers formed on the materials during air oxidation was produced when they were exposed to Ringer's solution. This effect was benefitial towards the improvement of the protection characteristics against corrosion of the oxide layers formed on the alloys. An average 10-fold increase of the resistance values was observed for exposures up to 1 week, though most of the improvement occurred already within the first 24 h. More compact layers resulted from such aging process. Next, the impedance modulus was observed to decrease during the exposure of the samples to Ringer's solution while they were left at their spontaneously-developed open circuit conditions, i.e. no polarization was applied to the systems. This effect is already noticeable from the observation of the EIS spectra given in Figure 2, and is more evident in the medium frequency range for the oxidized Zr25Ti alloy. Most of the change occurred already within the first 24 h. However, after one week of immersion time the R_{ox} of all three oxidized ZrTi samples remained high (around 10^6-10^7 Ω cm^2). The origin for the decrease in the values of R_{ox} during immersion may be related to the establishment of conductive electrolyte pathways inside pores existing in the oxide layers. The effect of alloy composition is also observed from the comparison of the resistance parameters obtained for each material. For the shortest exposure of 1 h, the R_{ox} value for the oxidized Zr45Ti alloy was approximately ten times higher than that determined for the oxidized Zr5Ti sample. The trend for R_{ox} with alloy composition is: Zr5Ti < Zr25Ti < Zr45Ti, and this agrees well with the observations obtained from the polarization data.

On the other hand, the impedance parameters related to the constant phase elements contained in the EC were almost invariant with the duration of the exposures of the samples to Ringer's solution. Though exponent values *n* smaller than 1 were always found, yet the values were greater than 0.8, an indication of a rather smooth surface for the passive oxide layers. Capacitance values for both the compact oxide layers and the electrolyte/oxide interfaces could be extracted from the CPE parameters using [32]:

$$C = \left(R^{1-n}Q\right)^{1/n} \qquad (2)$$

In this way, the order of magnitude of the capacitance values determined for both C_{ox} and C_{dl} were found to correspond to those typical for a compact barrier layer and for an interface at which charge transfer occurs, respectively.

3.2. Surface analysis of ZrTi alloy surfaces after air-oxidation treatment

The oxides present on the three ZrTi alloys after oxidation in air for 2 h at 500ºC were characterized using a combination of two analytical techniques (SEM/EDX and XRD) to obtain some information on the morphology and composition of the films. The scanning electron microscope photographs given in Figure 4 showed that the surface of the oxide layers was apparently rather flat, though different distributions of pores and cracks on their surfaces could be clearly observed for the different alloys. In this way, the surface of oxidized Zr5Ti exhibited many pores and cracks, whereas a uniform oxide layer was only observed on the surface of the oxidized Zr45Ti sample, and the oxidized Zr25Ti specimen exhibited an intermediate situation. This variation in the topography of the oxide layers between the oxidized alloys can also be observed from the inspection of the SEM images taken from cross sections through the oxide films (cf. Figure 5). The formation of an oxide layer on ZrTi alloys can be identified in these micrographs due to their lighter contrast in the SEM images. It is observed that the thickness of the oxide layer formed on the alloys as result of the oxidation process in air at 500 ºC during 2 h greatly diminishes for higher titanium contents in the ZrTi alloys. The thickest layer (ca. 250 μm) was formed on Zr5Ti, it amounted roughly a third in the case of Zr25Ti, and it was comparatively very thin on Zr45Ti (around 35 μm). Despite this great variation in thickness, the most striking difference between the oxide layers formed on the different alloys is related to their densities. A very dense and compact film occurred for oxidized Zr45Ti, whereas the oxide layers formed on the other alloys presented many defects and voids.

EDX analysis supports that the oxide layer becomes enriched in titanium (cf. Figure 6), whereas the XRD spectra displayed in Figure 7 demonstrate that TiO_2 and ZrO_2 are the only corrosion products resulting from air oxidation of the ZrTi alloys at 500 ºC. That is, no higher oxidation states for titanium and zirconium occur during the oxidation process for any of the ZrTi alloys.

Finally, Figure 8 presents the scanning electron micrographs of the three ZrTi samples after anodic polarization at +1.00 V_{SCE} in Ringer's solution at 37 ºC. There is no obvious variation in the surface morphologies of ZrTi samples as result of the anodic polarization tests compared to their condition prior to testing. This indicates that the anodic polarization tests had no major effect on the characteristics of the oxide layer of the ZrTi samples resulting from oxidation in air at 500 ºC for 2 hours.

4. Discussion and Conclusions

Experiments described in this work correspond to the electrochemical behaviour of previously oxidized ZrTi alloys in naturally-aerated Ringer's solution at 37 ºC. In this environment, these alloys are covered by an oxide film that was characterized using SEM, EDX and XRD.

The electrochemical behaviour of the oxidized ZrTi alloys corresponds to materials covered by oxide layers with barrier characteristics typical of a protective passive film. They are highly stable in Ringer's solution at 37 ºC, and the potential range for either localized corrosion or transpassivity lie well beyond the values that can be experienced in the human body. Indeed, no signs for passivity breakdown could be observed from the inspection of the linear polarization curves depicted in Figure 1, though the anodic potential limit was fixed at a high positive value (namely +1.00 V_{SCE}). The current densities related to the passive state of oxidized ZrTi alloys immersed in Ringer's solution at 37 ºC are 2-3 orders of magnitude smaller than those determined for the untreated alloys (see Figure 1 in reference [1]). The occurrence of metal dissolution through the passive layers has been decreased accordingly, which should greatly favour the biocompatibility of these materials as potential biomaterials for implant applications. Furthermore, alloys with low titanium contents such as Zr5Ti can also be considered for biomedical use after air oxidation at 500 ºC for 2 h, because the linear polarization curve for this material almost completely matches that determined for the untreated Zr45Ti alloy in the same environment, which was then regarded a good electrochemical characteristic for that material as to be considered for biomaterial application.

Tenacious and adherent oxide layers are produced on the ZrTi alloys by the air-oxidation procedure described in this work. The susceptibility to localized corrosion has been greatly reduced for the materials even for low titanium contents, and they remain practically unaffected both electrochemically and morphologically when subjected to rather high anodic potential values (cf. Figures 1, 4 and 8). High impedance values (around 10^6-10^7 Ω cm^2) were measured in the low frequency range of the spectra for all the oxidized ZrTi samples. This is an evidence of the rather high corrosion resistance of these materials in Ringer's solution at 37 ºC which has been conferred by the oxide layers formed during oxidation of the alloys in air at 500 ºC for 2 h. For all the oxidized ZrTi alloys, the impedance modulus values are 1 order of magnitude greater than the corresponding values for the untreated materials (cf. Figure 2 in ref. [1]. A more corrosion resistant oxide layer film has been thus formed during the oxidation pretreatment in air.

The impedance parameters in Table 3 can be employed to obtain estimates of the oxide film thickness. The procedure is based on the application of the parallel-plate capacitor model to these systems, as described by:

$$C = \frac{\varepsilon \varepsilon_0 A}{d} \qquad (3)$$

In order to determine the thickness of the oxide layer, d, the values of the dielectric constants of the oxides for each alloy, ε, would be required. Since those values could not be found in the scientific literature, the value $\varepsilon = 65$ for TiO_2 [33] was regarded to be an acceptable estimate at this time. A unity surface roughness factor was also adopted. The thicknesses of the oxide films formed on the different materials after air-oxidation at 500 ºC are given in Table 4. In general, these values are almost twice those determined for the untreated materials using the same procedure [1]. Therefore, thicker oxide layers are formed by the oxidation pretreatment on the oxidized ZrTi alloys than those spontaneously formed on these materials. On the other hand, these values are very similar for the three oxidized ZrTi alloys, and they are very thin compared to the surface films discovered using SEM from cross sections through the oxide films given in Figure 6. This feature strongly supports the use of a two-layer model to describe the electrochemical behaviour of the oxide films given by the equivalent circuit of Figure 3 [31]. Corrosion protection is mainly conferred to the alloys by the thin compact inner oxide layer, which amounts ca. 5 nm and directly in contact with the metallic crystalline lattice, whereas a less compact outer layer is formed film of the oxidized ZrTi alloy on top of it. From the comparison of the values of R_{ox} listed in Table 3, it can be concluded that the corrosion resistance of oxidized Zr45Ti sample was

better than for the oxidized Zr5Ti sample, and slightly better than oxidized Zr25Ti sample. This means that a relatively more compact and less porous inner TiO_2/ZrO_2 layer was formed on Zr45Ti sample for the oxidation treatments at 500 ^oC though the thickness is very similar in all the cases. As for the outer oxide layer, this was thickest for oxidized Zr5Ti, and the thinnest for oxidized Zr45Ti. Yet, this outer layer must not be very compact, and due to the occurrence of a distribution of pores and defects, the corrosion protection ability of the oxide film formed on ZrTi alloys almost exclusively depends on the characteristics of the inner layer, which effectively operates as a barrier film towards electron transfer reactions.

The increase of titanium contents in the alloys produces more corrosion resistant materials. Though this effect was already reported for the untreated alloys [1], it also applies to air-oxidized samples. Indeed, EDX data suggest that the passive oxide layers are enriched in titanium compared to the substrates, and XRD data indicate that they consist exclusively of mixed TiO_2/ZrO_2, without the occurrence of higher oxidation states of the metals.

Acknowledgments:

This work was supported by the Romanian CNCS Program, under project PN-II-ID-PCE-2011-3-0218, No. 266, and the Ministerio de Ciencia e Innovación (MICINN, Madrid, Spain) and the European Regional Development Fund (Brussels, Belgium) under Grant Number CTQ2012-36787. A Research Training Grant awarded to J.I. by the MICINN (*Programa de Formación de Personal Investigador*) is gratefully acknowledged. Thanks are due to Zirom S.A. (Giurgiu, Romania) for kindly providing the ZrTi alloys used in this work.

References:

1. G. Bolat, J. Izquierdo, J.J. Santana, D. Mareci, R.M. Souto, Electrochemical characterization of ZrTi alloys for biomedical applications, Electrochimica Acta 88 (2013) 447.
2. S. Rao, Y. Okazaki, T. Tateishi, T. Ushida, Y. Ito, Cytocompatibility of new Ti alloy without Al and V by evaluating the relative growth ratios of fibroblasts L929 and osteoblasts MC3T3-El cells, Materials Science and Engineering C 4 (1997) 311.

3. S. Piazza, G. Lo Biundo, M.C. Romano, C. Sunseri, F. Di Quatro, In situ characterization of passive films on Al-Ti alloy by photocurrent and impedance spectroscopy, Corrosion Science 40 (1998) 1087.
4. N.J. Hallab, S. Anderson, M. Caicedo, A. Brasherm K. Mikecz, J.J. Jacobs, Effects of soluble metals on human peri-implant cells, Journal of Biomedical Materials Research A 74 (2005) 124.
5. Y. Okazaki, E. Gotoh, Comparison of metal release from various metallic biomaterials in vitro, Biomaterials 26 (2005) 11.
6. R.J. Solar, Corrosion resistance of titanium surgical implant alloys: a review, in: B.C. Syrett, A. Acharya (Eds.), Corrosion and Degradation of Implant Materials, STP 684, American Society for Testing and Materials, Philadelphia, PA, 1979, p. 259.
7. R.W. Schutz, D.E. Thomas, Corrosion of titanium and titanium alloys, in: Metals Handbook, 9th ed., vol. 13, ASM International, Metals Park, OH, 1987, p. 669.
8. M.M. Lohrengel, Formation of ionic space charge layers in oxide films on valve metals, Electrochimica Acta 39 (1994) 1265-1271.
9. G.T. Burstein, R.M. Souto, Observations of localized instability of passive titanium in chloride solution, Electrochimica Acta 40 (1995) 1881.
10. R.M. Souto, G.T. Burstein, A preliminary investigation into the microscopic depassivation of passive titanium implant materials in vitro, Journal of Materials Science: Materials in Medicine 7 (1996) 337.
11. G.T. Burstein, C. Liu, R.M. Souto, The effect of temperature on the nucleation of corrosion pits on titanium in Ringer´s physiological solution, Biomaterials 26 (2005) 245.
12. G.T. Burstein, M. Carboneras, B.T. Daymond, The temperature dependence of passivity breakdown on a titanium alloy determined by cyclic noise thermammetry, Electrochimica Acta 55 (2010) 7860.
13. R.M. Urban, J.J. Jacobs, M.G. Tomlinson, J. Gavrilovic, J. Black, M. Peoc'h, Dissemination of wear particles to the liver, spleen, and abdominal lymph nodes of patients with hip or knee replacement, Journal of Bone and Joint Surgery A 82 (2000) 457.
14. I. Milošev, V. Antolič, A. Minovič, A. Cör, S. Herman, V. Pavlovčič, P. Campbell, Extensive metallosis and necrosis in failed prostheses with cemented titanium-alloy stems and ceramic heads, Journal of Bone and Joint Surgery 82B (2000) 352.
15. A.V. Rousslle, D. Heymann, D. Demais, C. Charrier, N. Passuti, M.F. Basle, Influence of metal ion solutions on rabbit osteoclast activities in vitro, Histology and Histopathology 17 (2002) 1025.

16. A. Balamurugan, S. Rajeswari, G. Balossier, A.H.S. Rebelo, J.M.F. Ferreira, Corrosion aspects of metallic implants - An overview, Materials and Corrosion 59 (2008) 855.
17. M. Niinomi, Recent research and development in titanium alloys for biomedical applications and healthcare goods, Science and Technology of Advanced Materials 4 (2003) 445.
18. S.Y. Yu, C.W. Brodrick, M.P. Ryan, J.R. Scully, Effects of Nb and Zr alloying additions on the activation behaviour of Ti in hydrochloric acid, Journal of the Electrochemical Society 146 (1999) 4429.
19. P. Marcus, On some fundamental factors in the effect of alloying elements on passivation of alloys, Corrosion Science 36 (1994) 2155.
20. J. Fahey, D. Holmes, T.-L. Yau, Evaluation of localized corrosion of zirconium in acidic chloride solutions, Corrosion 53 (1997) 54.
21. F. Rosalbino, D. Maccio, A. Saccone, E. Angelini, S. Delfino, Stability of the passive state of Zr-Nb crystalline alloys, Materials and Corrosion 63 (2012) 580.
22. G. Rondelli, B.Vicentini, Effect of copper on the localized corrosion resistance of Ni-Ti shape memory alloy, Biomaterials 23 (2002) 639.
23. M.C. García Alonso, L. Saldaña, G. Valles, In vitro corrosion behaviour and osteoblast response of thermally-oxidised Ti-6Al-4V alloy, Biomaterials 24 (2003) 19.
24. P. Kofstad, High Temperature Corrosion, 2nd ed., Ellis Horwood, 1986.
25. I. Saeki, H. Konno, R. Furuichi, The initial oxidation of type 430 stainless steel in O_2-H_2O-N_2 atmospheres at 1273 K, Corrosion Science 38 (1996) 19.
26. J. Pan, C. Leygraf, R.J. Petterson, J. Linden, Characterization of high temperature oxide films on stainless steels by electrochemical impedance spectroscopy, Oxid. Met. 50 (1998) 431.
27. C. Delgado-Alvarado, P.A. Sundaram Corrosion evaluation of Ti-48Al-2Cr-2Nb (at.%) in Ringer's solution, Acta Biomaterialia 2 (2006) 701.
28. S. Becker, A. Rahmel, M. Schorr, M. Schütze, Mechanism of isothermal oxidation of the intermetallic TiAl and of TiAl alloys. Oxid Met 38 (1992) 425.
29. J.W. Fergus, Review of the effect of alloy composition on the growth rates of scales formed during the oxidation of gamma titanium aluminide alloys, Materials Science and Engineering A 338 (2002) 108.
30. B. Yeum, Electrochemical impedance spectroscopy: Data analysis software; Echem Software, Ann Arbor, 2001.

31. J. Pan, D. Thierry, C. Leygraf, Electrochemical impedance spectroscopy study of the passive oxide film on titanium for implant application, Electrochimica Acta 41 (1996) 1143.
32. B.I. Wang, Y.F. Zheng, I.C. Zhao, Effects of Hf content and immersion time on electrochemical behavior of biomedical Ti-22Nb-xHf alloys in 0.9% NaCl solution Materials and Corrosion 60 (2009) 330.
33. J. Pan, D. Thierry, C. Leygraf, Electrochemical and XPS studies of titanium for biomaterial applications with respect to the effect of hydrogen peroxide, Journal of Biomedical Materials Research 28 (1994) 113.

Table 1.

Chemical composition of ZrTi alloys.

Sample	Composition / wt.%
Zr5Ti	Zr: 95, Ti: 5
Zr25Ti	Zr: 75, Ti: 25
Zr45Ti	Zr:55, Ti: 45

Table 2.

Electrochemical parameters determined from the linear potentiodynamic polarization curves measured for oxidized ZrTi alloys in aerated Ringer's solution at 37 ºC.

Sample	E_{corr} / V_{SCE}	j_{corr} / nA cm^{-2}	j_{pass} / μA cm^{-2}
Zr5Ti	-0.240	690	8.1
Zr25Ti	-0.285	210	1.7
Zr45Ti	-0.198	60	1.2

Table 3.

Impedance parameters of oxidized ZrTi alloys immersed in aerated Ringer's solution at 37 ^{o}C.

Sample	R_{ct} / kΩ cm^2	10^5 Q_{ct} / S cm^{-2} s^{-n}	n_{ct}	R_{ox} / MΩ cm^2	10^5 Q_{ox} / S cm^{-2} s^{-n}	n_{ox}
	After 1 h immersion in Ringer's solution					
Zr5Ti	3.5	3.1	0.82	4.4	0.6	0.85
Zr25Ti	2.3	3.4	0.81	3.5	0.7	0.84
Zr45Ti	2.1	3.4	0.80	2.9	0.7	0.84
	After 1 day immersion in Ringer's solution					
Zr5Ti	25.2	2.2	0.84	21.5	0.3	0.88
Zr25Ti	19.5	2.3	0.83	14.8	0.4	0.87
Zr45Ti	17.8	2.3	0.83	12.4	0.4	0.87
	After 1 week immersion in Ringer's solution					
Zr5Ti	36.1	2.1	0.85	43.1	0.2	0.89
Zr25Ti	32.4	2.2	0.84	41.5	0.2	0.89
Zr45Ti	28.3	2.2	0.83	39.3	0.2	0.88

Table 4.

Film thickness estimated from EIS results measured for oxidized ZrTi alloys in aerated Ringer's solution at 37 ^{0}C. A dielectric constant value of 65 was assumed in the calculation [33].

Sample	Film thickness / nm
Zr5Ti	5.78
Zr25Ti	4.80
Zr45Ti	4.98

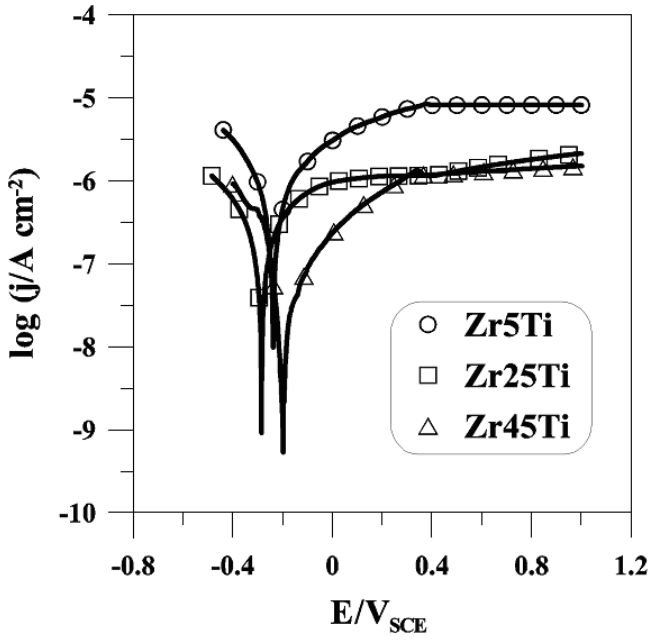

Figure 1. Linear potentiodynamic polarization curves for oxidized ZrTi samples immersed in aerated Ringer's solution at 37 ºC. Sweep rate: 1 mV s^{-1}.

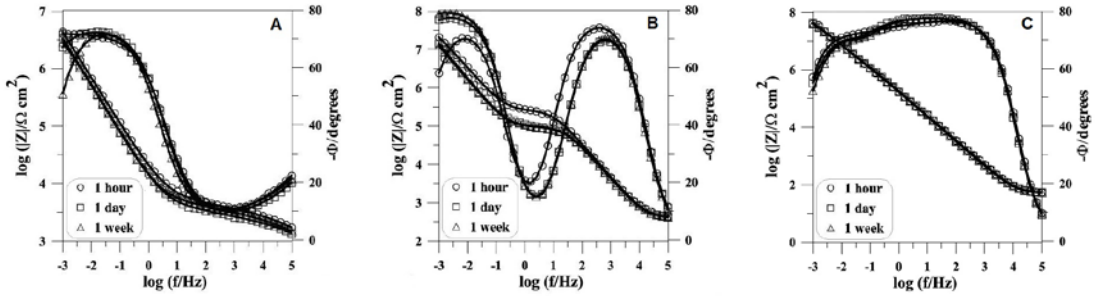

Figure 2.
Measured (discrete points) and fitted (solid lines) impedance spectra for oxidized ZrTi alloy samples recorded at their open circuit potentials during exposure to aerated Ringer's solution at 37 ºC: (A) Zr5Ti, (B) Zr25Ti, and (C) Zr45Ti. Exposure times are indicated in the plots.

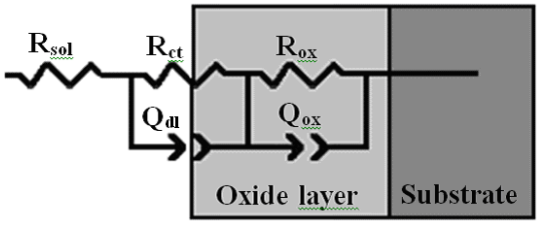

Figure 3.
Equivalent electrical circuit (EC) used for the interpretation of the impedance spectra measured for ZrTi alloys oxidized in air at 500 ºC for 2 h.

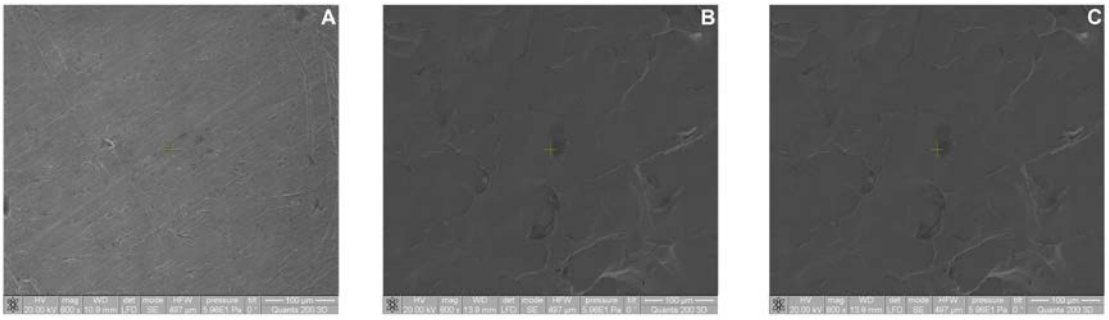

Figure 4.
SEM photographs of the oxidized ZrTi alloys as obtained from the oxidation process in air at 500 ºC for 2 h. (A) Zr5Ti, (B) Zr25Ti, and (C) Zr45Ti.

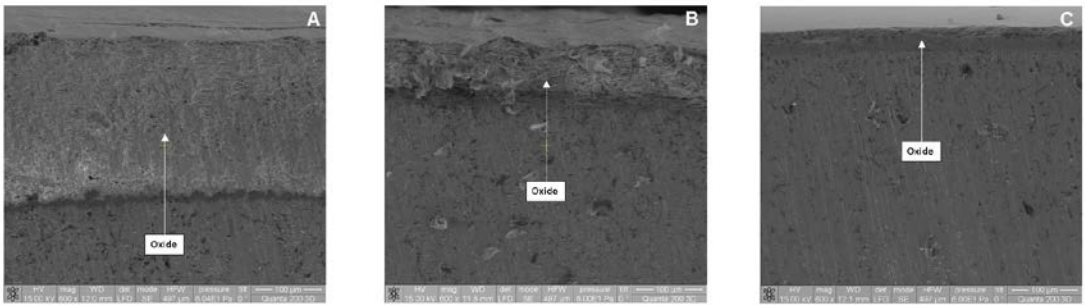

Figure 5.
SEM photographs of cross sections through the oxide film of the oxidized ZrTi alloys as obtained from the oxidation process in air at 500 ºC for 2 h. (A) Zr5Ti, (B) Zr25Ti, and (C) Zr45Ti.

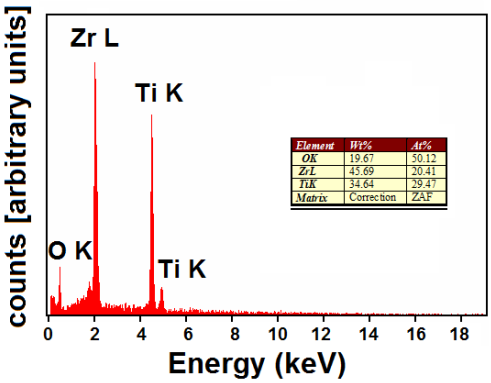

Figure 6.
EDX spectra measured at the surface of the oxidized Zr25Ti alloy as obtained from the oxidation process in air at 500 ºC for 2 h.

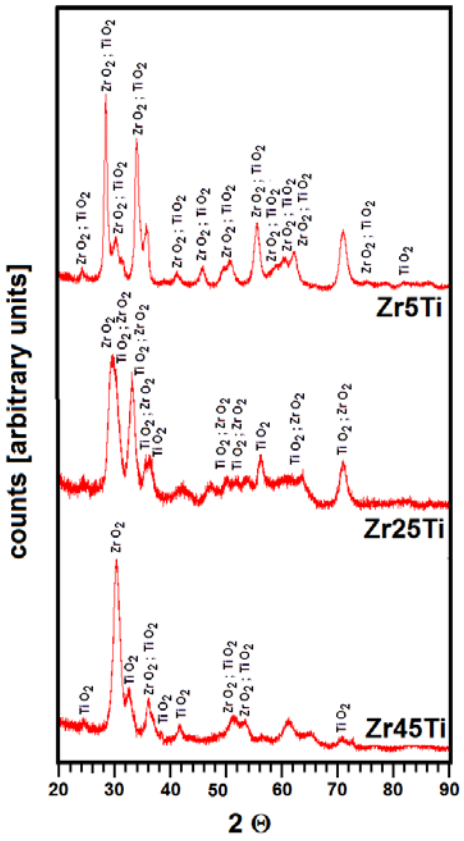

Figure 7.
X-ray difractograms of the oxidized ZrTi alloys as obtained from the oxidation process in air at 500 ºC for 2 h.

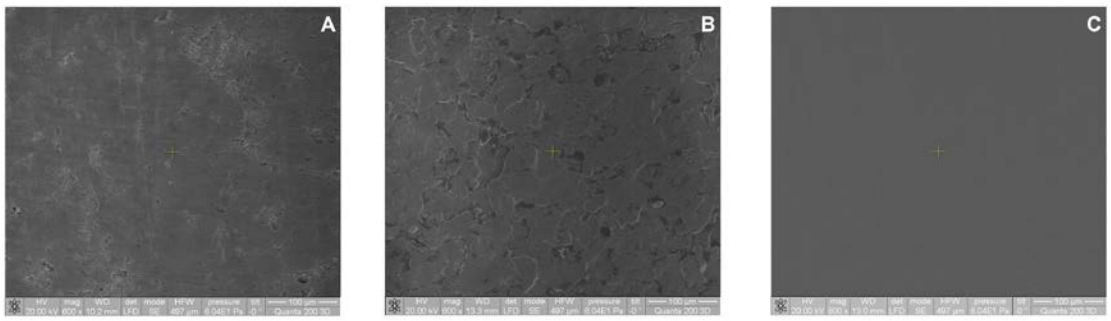

Figure 8.
SEM photographs of the oxidized ZrTi alloys retrieved from Ringer's solution at 37 ºC after recording the corresponding linear potentiodynamic polarization curves depicted in Figure 1. The samples were removed at the anodic potential value +1.00 V_{SCE}. (A) Zr5Ti, (B) Zr25Ti, and (C) Zr45Ti.